White microbeam diffraction from distorted crystals

R. Barabash, G. E. Ice,[a] B. C. Larson, G. M. Pharr, K.-S. Chung, and W. Yang
Metals and Ceramics and Solid State Divisions, Oak Ridge National Laboratory, Oak Ridge, Tennessee 37831-6118

(Received 10 April 2001; accepted for publication 7 June 2001)

We present a general description of white-beam (Laue) scattering from grains with dislocations. This approach is applied to examples with equal numbers of positive and negative Burger's vectors (paired) and with unpaired dislocations of one sign (geometrically necessary). We find that streaking of the Laue reflections is sensitive to both long-range geometrical rotations introduced by unpaired edge dislocations and to local rotation fluctuations introduced by the total number of dislocations (paired and unpaired). We demonstrate the technique by analyzing the dislocation distribution in a nanoindented Cu single crystal. [DOI: 10.1063/1.1389321]

The development of ultrabrilliant third-generation synchrotron x-ray sources[1,2] and recent progress in x-ray optics[3] has led to intense x-ray beams with submicron spatial resolution. Together with new instrumentation[4] it is now possible to use the Laue method to quantitatively determine elastic strain and local orientation (texture) distributions in individual grains or subgrains.[5,6] Here, we show from the general kinematic treatment of x-ray scattering by dislocations, how the dislocation structure of crystals can be measured with white beam microdiffraction.

A general kinematic treatment of x-ray scattering by crystals with dislocations was developed by Darwin,[7] Krivoglaz,[8] Warren,[9] Wilkens *et al.*,[10] and Thomson *et al.*[11] This approach is widely used for the analysis of dislocation density from powder diffraction measurements (Ungar *et al.*)[12] and is similarly applied to the analysis of dislocation substructure in single crystals by means of rocking curves.[13–15] The main disadvantage of the rocking curve technique is the need to rotate the sample; rotations introduce uncertainties in the real space coordinates of the scattering volume.[16] Laue white beam measurements however are performed with fixed sample orientation. Moreover with the Laue method, the intensity distributions near a large number of different reflections can be simultaneously analyzed from the same subgrain.

The precise shape of each Laue spot depends formally on the orientation of the grain/subgrain, the spectral distribution near the Bragg energy of the reflection, and the distribution of elastic and plastic deformation in the grain/subgrain. The momentum transfer corresponding to a Bragg/Laue reflection $\mathbf{G}_{hkl}$ we define as $\mathbf{k}_{hkl}-\mathbf{k}_0$, where $|\mathbf{k}_0|=|\mathbf{k}_{hkl}|=k$. Here, $\mathbf{k}_0$ is the incident wave vector and $\mathbf{k}_{hkl}$ is the scattered wave vector that satisfies the Bragg/Laue conditions. The diffuse scattering intensity depends on the deviation $\mathbf{q}=\mathbf{Q}-\mathbf{G}_{hkl}=\mathbf{k}-\mathbf{k}_{hkl}$ between the diffraction vector $\mathbf{Q}=\mathbf{k}-\mathbf{k}_0$, and the momentum transfer $\mathbf{G}_{hkl}$ for the Laue reflection (Fig. 1). With Laue diffraction the measured intensity I_L is a function of a vector $\mathbf{m}=\hat{\mathbf{k}}-\hat{\mathbf{k}}_{hkl}$ because of the radial integration through reciprocal space. The vector $\mathbf{m}$ is the difference between the unit vectors $\hat{\mathbf{k}}=\mathbf{k}/k$ and $\hat{\mathbf{k}}_{hkl}=\mathbf{k}_{hkl}/k_{hkl}$, that are defined by the direction of propagation of the scattered radiation. Here, $\mathbf{k}$ is the wave vector of the scattered intensity close to $\mathbf{k}_{hkl}$. To compare with Laue measurements, it is necessary to integrate the intensity distribution, $I(\mathbf{q})$ over the radiation wavelengths and to transform the reciprocal-space intensity distribution into its real-space projection at the charge coupled device (CCD) plane. The resulting intensity distribution can be written as:

$$I_L(\mathbf{m})=A\int I_0(k)I(\mathbf{q})dk, \tag{1}$$

$$\mathbf{q}=|\mathbf{k}_{hkl}|\mathbf{m}+\Delta k\mathbf{G}/|\mathbf{k}_{hkl}|;\quad \Delta k=|\mathbf{k}|-|\mathbf{k}_{hkl}|. \tag{2}$$

Here $I_0(k)$ is the intensity distribution of the white spectrum, $|k_{hkl}|$ is the radius of the Ewald sphere that passes through $\mathbf{G}_{hkl}$, and A is a constant. Equation (2) is valid when $\Delta k/|k_0|\ll 1$. The intensity distribution $I(\mathbf{q})$ of x-ray (or neutron) scattering due to dislocations can be computed from the expression.

$$I(\mathbf{Q})=\left|\sum_i f_i \exp[i\mathbf{Q}\times(\mathbf{R}_i^0+\mathbf{u}_i)]\right|^2,\quad \mathbf{u}=\sum_i c_t\mathbf{u}_{it}. \tag{3}$$

Here, f_i is the scattering factor from an individual atom i, with relaxed coordinates $\mathbf{R}_i=\mathbf{R}_i^0+\mathbf{u}_i$ due to the presence of

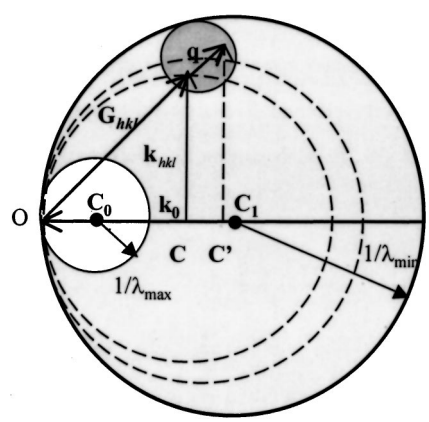

FIG. 1. For each wavelength, the center of the Ewald sphere (C) and the origin in reciprocal space (O) are separated by the distance 1/λ. This distance is different for each reflection *hkl* and corresponds to different Ewald spheres.

[a]Electronic mail: gei@ornl.gov

Downloaded 12 Mar 2002 to 128.219.47.178. Redistribution subject to AIP license or copyright, see http://ojps.aip.org/aplo/aplcr.jsp

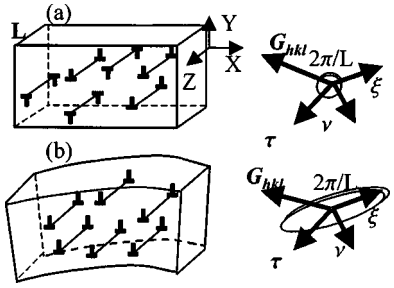

FIG. 2. Real and reciprocal space for crystals with: (a) an almost equal number of $+b$ and $-b$ dislocations and (b) an excess (geometrically necessary) $+b$ dislocations are shown.

defects, $\mathbf{u}_i$ is a total displacement from the equilibrium positions $\mathbf{R}_i^0$ corresponding to the crystal before deformation, and c_t is the random number.

Consider the set of edge dislocations illustrated in Fig. 2. All dislocations from this set have Burger's vectors, $\mathbf{b}_i$, parallel to the x axis and dislocations lines, τ parallel to the Z axis. The total displacement of this ith cell u_i due to all dislocations is defined by Eq. (3).

For an equal number of random ''$+\mathbf{b}$'' and ''$-\mathbf{b}$'' dislocations [Fig. 2(a)], the average deformation tensor is negligible and broadening of the diffuse scattering is induced by random local fluctuations in the unit cell orientations and d spacing that tend to cancel out over long length scales. Coherence is not changed along the direction of dislocation lines τ, and the diffuse intensity in this direction is the same as for crystals without dislocations. Perpendicular to τ, the diffuse distribution is roughly symmetric with a characteristic half width dependent on the total dislocation density n; $2\delta \propto \sqrt{n}$.[8,14]

For excess dislocations [Fig. 2(b)], the dislocation density tensor can be written in terms of the antisymmetric Levi–Civita tensor of third rank $\varepsilon_{\tau lm}$ and a dislocation density tensor of second rank $\rho_{\tau n}$.[2,17–18]

$$\varepsilon_{\tau lm}\left(\frac{\partial \omega_{mn}}{\partial x_l}\right) = -\rho_{\tau n}. \tag{4}$$

From Eq. (4), it follows that there are only two nonzero components of the mean deformation tensor: $\omega_{xy} = -\omega_{yx} = n^+ bx$. This distortion field represents a pure rotation about the Z axis that increases with displacement in x.

The unpaired-dislocation-induced diffuse scattering near a Laue spot can be qualitatively understood along three characteristic directions. In the radial direction, x-ray scattering is primarily sensitive to dilatational changes in the lattice. Local strain fields around dislocations can introduce such changes, but Laue diffraction is inherently insensitive to scattering variations in the radial direction; energy scans are needed to probe these changes. In the transverse direction, we define two natural axes ξ and ν. The axis ξ is defined as perpendicular to both the radial direction, $\mathbf{g} = \mathbf{G}_{hkl}/G_{hkl}$, and to the axis τ. The second axis ν is defined as perpendicular to the ξ axis and to $\mathbf{g}$. With this coordinate system, the diffuse scattering is strongly elongated in the ξ direction, and depends on the relative orientation between the active dislocation system, the momentum transfer unit vector $\mathbf{g}$, and the penetration depth L.

To illustrate the dependence of the Laue intensity distribution on the penetration depth (L) covered by the beam passing through the sample, we simulated Laue contour maps for different values of L keeping a constant total value of excess dislocations in the whole scattering region (Fig. 3). The simulations show that this dislocation system results in a rod-like intensity distribution (Fig. 3) around the (222) reflection. The major axis is located in the plane (111) parallel to the direction ξ=[213]. The character of the intensity distributions along the ξ, and ν axes is different as expected [Fig. 3(b)]. The intensity distribution along the ξ axis has a flat-top shape with a huge full width at half maximum (FWHM). Along the ν axis, it is a narrow Gaussian function and is sensitive to dislocation density. With L, the penetration

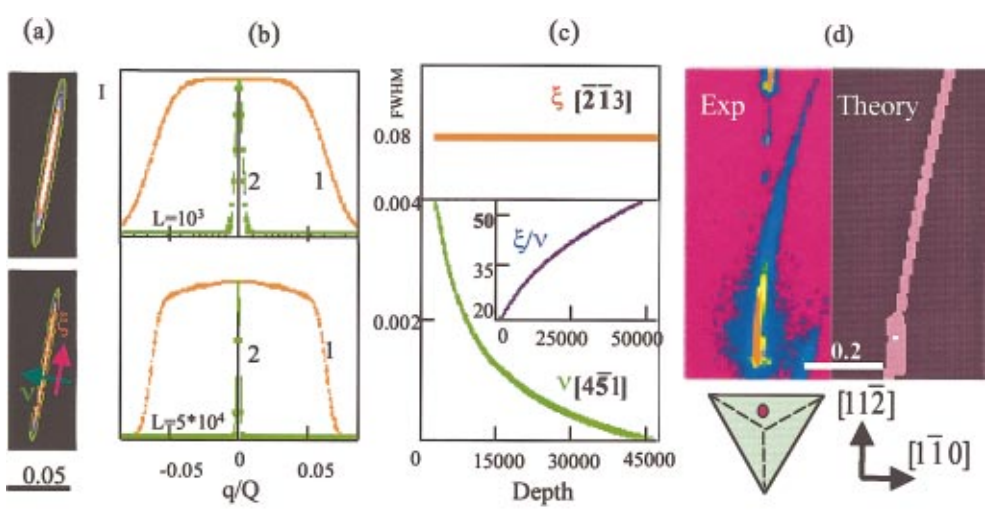

FIG. 3. (Color) Contour maps around the reflection (222) for $L^* n^+ =$ constant and $L_2 = 50\ L_1$ (a), intensity distributions along the axis ξ (1) and ν (2) (b), FWHM along ξ and ν directions with their ratio (insert) as a function of L (c), and experimental (left-hand side) and simulated (right-hand side) Laue images of the (222) reflection in the CCD plane for a nanoindented Cu single crystal (red point—position of the beam on the indentation) (d) are shown. The orientation of the dislocation system in this simulation corresponds to Burger's vector parallel to [011], a dislocation line parallel to [211], and total dislocation density $n = 2\times 10^{11}$ cm^{-2} with an excess dislocations density $n^+ = 0.5\ n$. To model the vertical (red) part of the image, a second slip system with Burger's vector parallel to [101] and dislocation line parallel to [121] was required.

Downloaded 12 Mar 2002 to 128.219.47.178. Redistribution subject to AIP license or copyright, see http://ojps.aip.org/aplo/aplcr.jsp

length in interatomic spacings, the FWHM along the ξ directions [Fig. 3(c) red] is insensitive to L if total number of excess dislocations along the L is constant, $L*n^{+} = \text{constant} \gg 0.1\sqrt{n}$. In the ν direction [Fig. 3(c) green], the FWHM decreases (as the dislocation density decreases). This means that the total dislocation density can be determined from the intensity distribution along the ν direction, while the total number of excess dislocations, can be obtained from the intensity distribution along the ξ direction.

Microbeam-Laue measurements of deformation in a nanoindented Cu single crystal are used to illustrate the application of the x-ray micro-Laue technique for the analysis of dislocation structure. The Cu single crystal surface normal was parallel to [111]. The corresponding coordinate axes around the indentation are shown in Fig. 3(d). Laue images were taken at various positions in the pyramidal indentation. One experimental image (pink) reveals long streaks with distinctive orientations relatively to the indentation. These streaks have been qualitatively discussed previously.[4] We have simulated the Laue contour maps corresponding to different arrangements of the primary excess dislocations. The plastic response of a material, subjected to indentation can be understood by the formation of excess or ''geometrically necessary'' dislocations that appear in the material to accommodate the indentor.[19] Deformation changes character as the beam penetrates the sample. A comparison to the experimental data is shown in the black field of Fig. 3(d). The elongation direction can be modeled with one system in the weak tail but requires two systems near the intensive (red) portion of the streak. This portion of the Laue streak might also be formed due to dislocations with Burger's vector [110] in the slip plane (001). However, an analysis of the FWHM in the direction perpendicular to the central portion of the streak favors the previously discussed two dislocation systems. Comparison to experimental data makes it possible to determine the orientation of the dislocation line τ, the Burger's vectors **b**, and the normal to the slip plane of the primary dislocation set.

In summary, we developed a formalism for calculating white-beam Laue diffraction patterns for distributions of dislocations in crystals and we have shown that such calculations can be used to obtain quantitative information on active dislocation systems in deformed materials.

This research was sponsored by the Division of Materials Sciences and Engineering, Office of Basic Energy Sciences, and the U.S. Department of Energy under Contract No. DE-AC05-00OR22725 with UT-Batelle, LLC.

[1] B. Buras and S. Tazari, *European Synchrotron Radiation Facility Report of European Synchrotron Radiation Project*, Cern LEP Division, Geneva, Switzerland (1984).
[2] G. K. Shenoy, P. J. Viccaro, and D. M. Mills, *Characteristics of the 7 GeV Advanced Photon Source: A Guide for Users* (Argonne National Laboratory, Argonne, IL, 1988), N.ANL-88-9.
[3] G. E. Ice, X-Ray Spectrom. **26**, 315 (1997).
[4] B. C. Larson, N. Tamura, J. S. Chung, G. Ice, J. D. Budai, J. Z. Tischler, W. Yang, H. Weiland, and W. P. Lowe, Mater. Res. Soc. Symp. Proc. **590**, 247 (2000).
[5] M. A. Marcus, A. A. Macdowell, E. D. Isaacs, K. Evans-Lutterodt, and G. Ice, Mater. Res. Soc. Symp. Proc. **428**, 545 (1996).
[6] J. S. Chung, N. Tamura, G. Ice, B. C. Larson, and J. D. Budai, Mater. Res. Soc. Symp. Proc. **563**, 169 (1999).
[7] C. Darwin, Philos. Mag. **27**, 315 (1914); **43**, 800 (1922).
[8] M. Krivoglaz, *X-Ray and Neutron Diffraction in Nonideal Crystals* (Springer, Berlin, 1996).
[9] B. Warren, *X-Ray Diffraction* (Dover, New York, 1969).
[10] M. Wilkens, Phys. Status Solidi A **2**, 359 (1970); *Fundamental Aspects of Dislocation Theory II*, pp. 1195–1221, edited by J. A. Simmons, R. de Wit, and R. Bullough (National Bureau Standards Special Publ. 317, Washington D.C., 1970), II, pp. K1–K7.
[11] R. Thomson and L. E. Levine, Acta Crystallogr., Sect. A: Found. Crystallogr. **A53**, 590 (1997).
[12] T. Ungar, H. Mughrabi, D. Ronnpagel, and M. Wilkens, Acta Metall. **32**, 333 (1984).
[13] R. Barabash and P. Klimanek, J. Appl. Crystallogr. **32**, 1050 (1999).
[14] R. Barabash and P. Klimanek, Z. Metallkd. **92**, 70 (2001).
[15] O. Castelnau, T. Chauveau, M. Drakopoulos, A. Snigirev, I. Snigireva, C. Schroer, and T. Ungar, Mater. Sci. Forum **347**, 297 (2000).
[16] J. S. Chung and G. Ice, J. Appl. Phys. **86**, 5249 (1999).
[17] L. Landau and E. Lifshitz, *Theory of Elasticity* (Pergamon, Oxford, 1959).
[18] G. Arfken, *Mathematical Methods for Physicists* (Academic, New York, 1970).
[19] A. Gouldstone, H.-J. Koh, A. Giannakopulus, and S. Suresh, Acta Mater. **48**, 2277 (2000).

Downloaded 12 Mar 2002 to 128.219.47.178. Redistribution subject to AIP license or copyright, see http://ojps.aip.org/aplo/aplcr.jsp